

GPS code phase variations (CPV) for GNSS receiver antennas and their effect on geodetic parameters and ambiguity resolution

Tobias Kersten¹  · Steffen Schön¹

Received: 3 April 2016 / Accepted: 8 December 2016 / Published online: 24 December 2016
© Springer-Verlag Berlin Heidelberg 2016

Abstract Precise navigation and geodetic coordinate determination rely on accurate GNSS signal reception. Thus, the receiver antenna properties play a crucial role in the GNSS error budget. For carrier phase observations, a spherical radiation pattern represents an ideal receiver antenna behaviour. Deviations are known as phase centre corrections. Due to synergy of carrier and code phase, similar effects on the code exist named code phase variations (CPV). They are mainly attributed to electromagnetic interactions of several active and passive elements of the receiver antenna. Consequently, a calibration and estimation strategy is necessary to determine the shape and magnitudes of the CPV. Such a concept was proposed, implemented and tested at the Institut für Erdmessung. The applied methodology and the obtained results are reported and discussed in this paper. We show that the azimuthal and elevation-dependent CPV can reach maximum magnitudes of 0.2–0.3 m for geodetic antennas and up to maximum values of 1.8 m for small navigation antennas. The obtained values are validated by dedicated tests in the observation and coordinate domain. As a result, CPV are identified to be antenna-related properties that are independent from location and time of calibration. Even for geodetic antennas when forming linear combinations the CPV effect can be amplified to values of 0.4–0.6 m. Thus, a significant fractional of the Melbourne–Wübbena linear combination. A

case study highlights that incorrect ambiguity resolution can occur due to neglecting CPV corrections. The impact on the coordinates which may reach up to the dm level is illustrated.

Keywords GNSS receiver antenna calibration · Code phase variation · Group delay variation · Carrier phase centre correction · GPS/GNSS antennas · Melbourne–Wübbena linear combination · Ambiguity resolution

1 Introduction

GNSS receiver antennas are designed to have an omni-directional and stable radiation pattern to receive reliably all signals from the upper hemisphere (Kaplan 1996; Petrovski and Tsujii 2012). As every GNSS antenna is a compromise between weight, size, gain and field of application, and therefore antenna radiation pattern, it will never be possible to design a perfect antenna that fits all requirements named above at the same level (Engheta and Ziolkowski 2006; Rao et al. 2013). This means that (1) far- and near-field environmental conditions (pillars, mountings, etc.) influence the reception properties (Schupler 2001) and (2) that antennas of the same type show differences in the reception properties. Several publications underline that this is still critical nowadays (Kaniuth and Stuber 2002; Wanninger 2009; Aerts 2011; Aerts et al. 2013; Aerts and Moore 2013; Tatarnikov and Astakhov 2013; Schmid 2013).

For carrier phase observations, the properties of the receiver antenna and their impact on geodetic parameters have been studied since the beginning of the geodetic use of GPS and later GNSS, as indicated by studies from Sims (1985) and Geiger (1988). Besides chamber calibrations (Schupler and Clark 1991, 2001; Görres et al. 2006; Zeimet 2010), field methods based on the currently available GNSS

Disclaimer The authors do not recommend any of the products used within this study. Commercial products were named for scientific transparency. Please note that a different receiver/antenna unit of the same manufacturer and type may show slightly different characteristics.

✉ Tobias Kersten
kersten@ife.uni-hannover.de

¹ Institut für Erdmessung, Leibniz Universität Hannover, Schneiderberg 50, 30167 Hannover, Germany

signals are in use. Approaches to determine the GPS carrier phase centre corrections (PCC) relative to a reference antenna (Allan Osborne AOAD/M_T) have been developed by Mader and MacKay (1996) or Mader (1999), known as *relative calibration*. Obtained corrections (relative PCC) have been necessary, e.g. to combine GPS with other space geodetic observation techniques like Very Long Baseline Interferometry (VLBI) and Satellite Laser Ranging (SLR) to obtain a consistent realisation of the International Terrestrial Reference Frame (ITRF) or to improve other precise GPS approaches.

Absolute calibration of GPS antennas, i.e. calibrations independent from a reference antenna and geographic location of calibration, was developed by Institut für Erdmessung (IfE), Leibniz Universität Hannover in close cooperation with Geo++[®] during joint research projects (Wübbena et al. 1996, 2000, Seeber et al. 1997a; Böder et al. 2001; Seeber and Böder 2002). This approach is nowadays state of the art and an international standard (Hannover concept of absolute antenna calibration) in the International GNSS Service (Schmid et al. 2016). The antenna working group publishes updates of the absolute PCC (Schmid 2016; Schmid et al. 2016) for receiver and satellite antennas in the antenna exchange format ANTEX (Rothacher and Schmid 2010) which contains type mean values of all relevant antennas. In addition to type mean values from the IGS, the European Permanent Network (EPN) provides PCC from individual calibrations for some receiver antennas.

The switch from relative to absolute antenna calibration values, initially applied by the ITRF2005 (Schmid et al. 2005; Steigenberger et al. 2007), improved the consistency between products from GNSS, VLBI and SLR significantly by about 0.6 ppb (height change averages of about 4 mm) and thus improves the generation of later realisations of the ITRF (Altamimi et al. 2016). Furthermore, PCC are mandatory for GNSS-based time and frequency dissemination (Ray and Senior 2003, 2005; Defraigne and Petit 2003) or real-time kinematic networks.

Antenna-related studies were mainly focused on carrier phase observations. Code phase variations have been of minor interest in geodesy, mainly due to the pronounced code noise level. Variations of the code phase are discussed especially within the GNSS antenna design in the electro-technical literature. Kunysz (1998) proposed group delay variations (GDV) as an instrumental-related effect which is induced by the variation of the phase with frequency, a common formulation in the electro-technical literature. Rao et al. (2013) consider that these GDV are also a function of elevation and azimuth. However, a clear distinction between CPV and GDV is still missing.

In contrast to geodetic applications, safety-critical navigation, e.g. precision landing approaches (RTCA 2006;

Murphy et al. 2007; Kube et al. 2012), requires accurate and well-known antenna reception properties for code phase observations, too. Consequently, elevation- and azimuth-dependent variations of the code phase have been investigated for receiver antennas. These studies are strengthened by numerical analyses from van Graas et al. (2004), Kim (2005) and Dong et al. (2006) with additional practical applications described, e.g. in Haines et al. (2012) and Wirola et al. (2008). Wübbena et al. (2008) determined CPV based on the absolute antenna calibration with a robot in the field, using the currently available signals in space. This concept uses undifferentiated observations in a real-time process (Kalman filter) to estimate the CPV. However, neither the used model nor analytical studies are published expect a roughly explained basic concept in Wübbena et al. (2008) and Rao et al. (2013).

In addition to code-based navigation, CPV are needed for any GNSS processing strategy where carrier and code phases are combined, e.g. ambiguity resolution or time transfer. For a cycle slip detection and ambiguity resolution independently of geometry and baseline length, the Melbourne–Wübbena linear combination (MW-LC) (Melbourne 1985; Wübbena 1985) is a common and prominent method. Since code observations on both frequencies are combined in the MW-LC, the effect of CPV on individual frequencies can be amplified by the linear combination and can lead to incorrectly solved MW ambiguities.

In this paper, we will focus on the effect on the measurements rather than on an electro-technical explanation. Thus, we will use the term code phase variations (CPV) to be consistent to the PCC definition which is justified by the synergy of carrier and code phase observation (Hatch 1982). The remainder of the paper is structured as follows. In Sect. 2, we present our method to determine CPV in a post-processing approach, based on the Hannover concept of absolute antenna calibration. Next, the obtained CPV are presented for different exemplary but typical antenna types. We demonstrate that some antennas will have pronounced CPV of up to 1.8 m that influences precise coordinates. In Sect. 4, short baseline common clock experiments are reported to validate the obtained CPV at the single difference level and to affirm the antenna-related characteristic of CPV. Single point positioning results are used to show the improvement in accuracy when applying CPV. Finally, in Sect. 5 the impact on ambiguity resolution is investigated when using Melbourne–Wübbena linear combination.

2 Definition and estimation of receiver antenna CPV

2.1 Geometrical definition of CPV

GPS CPV have been identified to be a specific property of receiver antennas, strongly varying with the antenna design

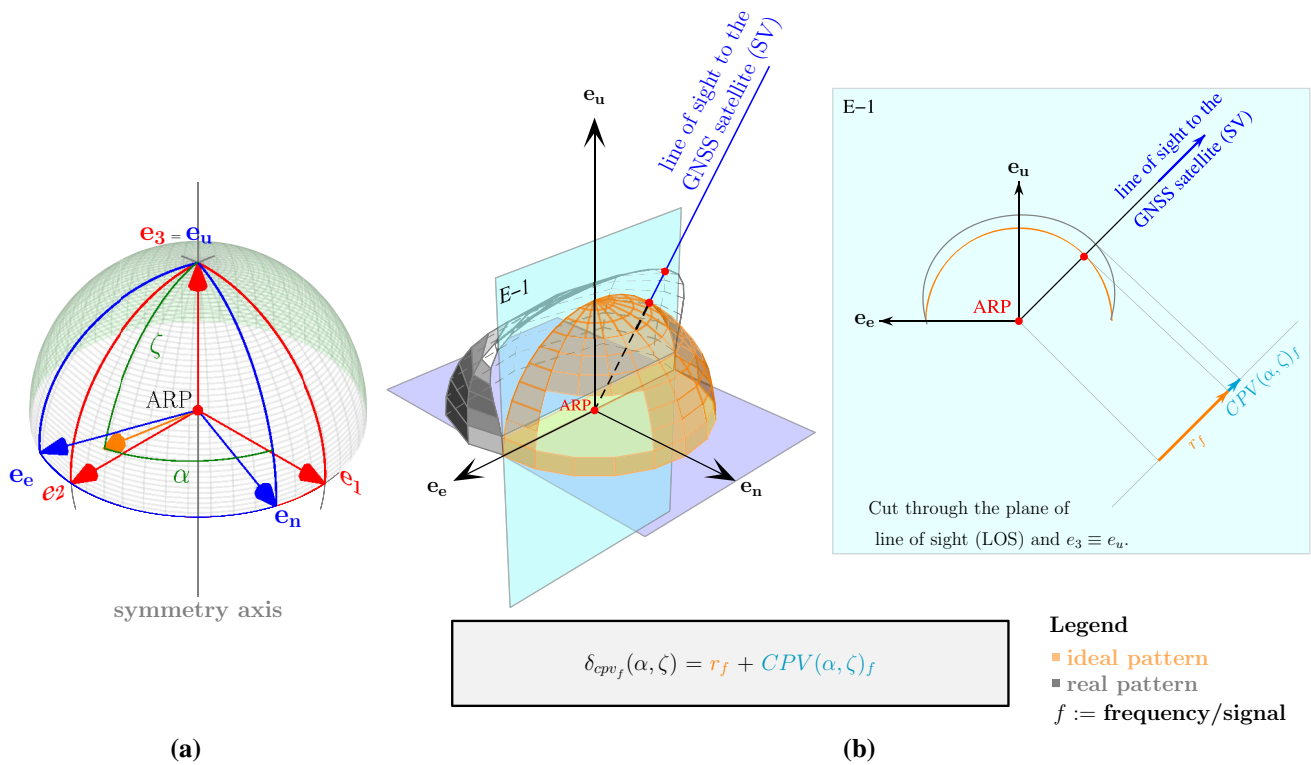


Fig. 1 Definition of Code Phase Variations (CPV) of GNSS receiver antennas, **a** definition of the antenna body frame ($[e_1 \ e_2 \ e_3]^T$) and relation to the topocentric coordinate system ($[e_n \ e_e \ e_u]^T$), **b** definition of CPV along the line-of-sight (LOS) to a specific satellite

(Rao et al. 2013; Dong et al. 2006). Although the combination of receiver, antenna and cable has to be taken into account, since they are not independent from each other, the antenna is the driving factor. We define our parametrisation of CPV, as well as PCC, in a left-handed antenna body frame, cf. Fig. 1a.

Its origin coincides with the antenna reference point (ARP). The ARP is defined by convention. For most of the GNSS receiver antennas, this is the lowest point of the 5/8" adaptor located in the vertical symmetry axis (Kouba 2009). However, a very small amount of antennas have a different definition, e.g. LEIAT303/503, AOAD/M_B or any Trimble antenna (TRM*), used with the Trimble conical weather radome (TCWD) where an additional ground-plane affects the ARP definition (IGS 2016a,b). Special definitions of the ARPs have to be considered appropriately.

The (vertical) symmetry axis, which is mostly the antenna boresight direction, defines the $[e_3]$ vector of the antenna body frame. Perpendicular to $[e_3]$, the $[e_1]$ vector is defined. By convention (Kouba 2009; Rothacher and Schmid 2010; Schmid et al. 2016), either a special north mark (special label, mark, display) or the high-frequency (HF) connector at the GNSS antenna materialise this direction. Finally, $[e_2]$ completes the left-handed system. The antenna body frame $[e_i]^T$ only coincides with a topocentric coordinate system ($[e_n \ e_e \ e_u]^T$) in static applications if the antenna

is levelled and orientated to north. In this well-defined coordinate system, PCC or CPV are parametrised by an azimuth angle α and a zenith angle ζ as depicted in Fig. 1a.

GNSS receiver antennas are designed to provide an omnidirectional radiation pattern (Kaplan 1996; Huang and Boyle 2008; Rao et al. 2013). Deviations from such an ideal hemispherical pattern are known in the literature for carrier phases as phase centre variations (PCV) (Sims 1985; Mader and MacKay 1996; Wübbena et al. 1996). A consistent set of PCC is composed of PCV and their related carrier phase centre offsets (PCO). In analogy to PCC, Eq. (1) defines the parametrisation of CPV. For each individual frequency f , the CPV correction $\delta_{CPV_f}^j$ has to be added to the pseudorange observation as a function of α and the zenith angle ζ along the line-of-sight (LOS) to the GNSS satellite j ,

$$\delta_{CPV_f}^j(\alpha, \zeta) = r_f + CPV(\alpha, \zeta)_f. \tag{1}$$

Due to the pseudorange character of GNSS observations, the radius of the sphere r_f is an unknown value and cannot be estimated. This is true for CPV and PCC as well. Since this parameter is constant, it acts like an unknown offset, so that its value does not matter for practical applications since it will be absorbed in a receiver clock component during GNSS processing.

2.2 Estimation of CPV with spherical harmonics

An useful and typical mathematical formulation for the parametrisation of CPV is the separation into functions depending only on azimuth $g_f(\alpha)$ and only on zenith angle $h_f(\zeta)$ in the antenna body frame,

$$\delta_{\text{CPV}_f}^j = g_f(\alpha) \cdot h_f(\zeta) \quad \text{with} \quad \begin{cases} 0 \leq \alpha \leq 2\pi \\ 0 \leq \zeta \leq \pi/2 \\ f := \text{GNSS frequency} \end{cases} \quad (2)$$

which are modelled by a system of continuous, spherical harmonic (SH) functions as described, for example, in [Hobson \(1931\)](#) and [Hofmann-Wellenhof and Moritz \(2006\)](#). This is a common procedure in geodetic as well as electro-technical literature ([Huang and Boyle 2008](#)).

The CPV are expanded by a double summation of the unknown coefficients A_n^m and B_n^m ,

$$g_f(\alpha) \cdot h_f(\zeta) = A_0^0 + \sum_{n=1}^{n_{\max}} \sum_{m=1}^{m_{\max}} \{ A_n^m C_n^m(\alpha, \zeta) + B_n^m S_n^m(\alpha, \zeta) \}. \quad (3)$$

with the maximum degree n_{\max} and order m_{\max} of the spherical expansion. The coefficients $C_n^m(\alpha, \zeta)$ and $S_n^m(\alpha, \zeta)$ are defined by the products of sine and cosine and the associated Legendre functions P_n^m ,

$$\begin{cases} C_n^m(\alpha, \zeta) \\ S_n^m(\alpha, \zeta) \end{cases} = P_n^m(\cos \zeta) \cdot \begin{cases} \cos m\alpha \\ \sin m\alpha \end{cases}. \quad (4)$$

An optimal set of SH coefficients A_n^m and B_n^m has to be estimated. The final solution of the estimation process (the CPV pattern) is determined by a SH synthesis.

2.3 Modelling the code phase observations

The CPV are estimated in a least-squares adjustment with time-differenced receiver-to-receiver single differences (RRSD) from a very short baseline (approx. 7 m distance) being the observations. The antenna under test is installed at one endpoint A of the baseline on a robot that can rotate and tilt the antenna in a fixed point. The second endpoint B is static.

The observations are obtained as follows: Starting with the code observation $P_{A_f}^j$ between a station A and a satellite j per frequency f ,

$$P_{A_f}^j = \rho_{A_f}^j + C_{A_f}^j + D_{A_f}^j + S_{A_f}^j + \epsilon_{A_f}^j \quad (5)$$

with the geometrical distance $\rho_{A_f}^j$ between satellite and receiver and the groups of combined errors:

- $C_{A_f}^j$: clock corrections and constant delays,
- $D_{A_f}^j$: distance-dependent effects,
- $S_{A_f}^j$: station (satellite and receiver)-related effects,

as well as the sum of unmodelled effects, combined in an additional variable $\epsilon_{A_f}^j$. To complete Eq. (5), the combined errors for the clock parameters are defined by

$$C_{A_f}^j = c \cdot (\delta t_A - \delta t^j) + d_{A,f} - d_f^j, \quad (6)$$

with the satellite and receiver clock corrections wrt. GPS system time δt^j and δt_A , the sum of hardware delays $d_f^j, d_{A,f}$ (due to different receiver boards, internal cable delays, etc.) of both, the satellite and the receiver. The distance-dependent effects are collected by

$$D_{A_f}^j = \delta_{\text{iono}_{A,f}}^j + \delta_{\text{tropo}_A}^j + \delta o^j + \delta_{\text{rel}_A}^j, \quad (7)$$

with the delays $\delta_{\text{iono}_{A,f}}^j$ and $\delta_{\text{tropo}_A}^j$ caused by ionospheric and tropospheric refraction, respectively, the orbit errors δo^j and the relativistic effect $\delta_{\text{rel}_A}^j$. Finally, all satellite- and receiver-dependent errors are collected by

$$S_{A_f}^j = \text{CPV}_{A,f} + \delta_{\text{mp}_{A,f}} + \text{CPV}_f^j + \delta_{\text{mp}_f}^j, \quad (8)$$

with the code phase variations $\text{CPV}_{A,f}$ and CPV_f^j at the ground station and satellite, respectively, as well as far-field multipath at both antennas ($\delta_{\text{mp}_{A,f}}, \delta_{\text{mp}_f}^j$).

To reduce the majority of error components of the code observations, single differences $P_{AB_f}^j(\alpha, \zeta, t_i)$ between the two stations A and B (RRSD), which are spatially very close to each other (approx. 7 m), are formed at every epoch t_i to each satellite j and for every frequency f

$$\begin{aligned} P_{AB_f}^j(t_i) &= P_{B_f}^j(t_i) - P_{A_f}^j(t_i) \\ &= \rho_{AB_f}(t_i) + C_{AB_f}^j(t_i) + D_{AB_f}^j(t_i) \\ &\quad + S_{AB_f}^j(t_i) + \epsilon_{AB_f}(t_i) \end{aligned} \quad (9)$$

with the differential distance depending parts collected in $D_{AB_f}^j(t_i)$, the differential clock corrections and delays in $C_{AB_f}^j(t_i)$, the differential station-related effects including CPV in $S_{AB_f}^j(t_i)$ and the noise $\epsilon_{AB_f}(t_i)$.

Based on Eq. (9), four additional steps and assumptions are necessary for the CPV determination approach developed at IfE (cf. Table 1):

1. Thanks to a very short baseline, distance-dependent effects (i.e. troposphere, ionosphere and orbit errors) are reduced to an insignificant level by RRSD as well as hardware delays and CPV at the satellite are eliminated

Table 1 Reduction in individual error sources in the post-processing approach of CPV determination

Error term	Effect	Characteristic	Method of reduction
$\delta t_A, \delta t_B$	Receiver clock	Identical drift due to common clock	SD, TD
$CPV_{A,B}$	Code phase variations	Azimuth/elevation dependent	TD
δ_{mp}	Multipath	Azimuth/elevation dependent	TD
d_A^j, d_B^j	Signal delay	Constant	TD
$\delta_{tropo_A}, \delta_{tropo_B}$	Troposphere	Distance/elevation dependent	SD on a very short baseline (7 m)
$\delta_{iono_A}, \delta_{iono_B}$	Ionosphere	Distance/elevation dependent	SD on a very short baseline (7 m)
$\delta_{rel_A}^j, \delta_{rel_B}^j$	Relativistic effect	Distance dependent	Model (Kouba 2004), SD on a very short baseline
$\Delta \rho_{AB}^j$	Diff. geometric range	Variable	Robot Motion Model

SD single differencing, TD time differencing

2. If a common clock set-up is used, i.e. if the receivers are linked to the same external frequency standard, the differential receiver clock correction $\delta t_{AB}(t_i)$ is constant at least within a time span of smaller than some seconds. In our approach, both individual receivers are connected to one external frequency reference (cf. Sect. 2.5).
3. In order to eliminate the impact of CPV at station B , time differences are formed. A rotation of the antenna under test between epochs is needed to preserve the interesting information about its CPV. The time span five seconds is the longest period; the antenna calibration unit needs to change the orientation of the antenna under test. In general, this time span is not longer than one second. Thus, further station-dependent errors (especially multipath) are reduced considerably which has been verified by Wübbena et al. (1997), Seeber et al. (1997b) or Böder et al. (2001). The hardware delays are eliminated as well as the differential receiver clock correction.
4. A precise robot motion model provides information to correctly determine the geometric delay $\Delta \rho_{AB_f}^j(\alpha_i, \zeta_i, \alpha_{i+1}, \zeta_{i+1})$. Finally, the time-differenced RRSd $\Delta P_{AB_s}^j(t_i, t_{i+1})$ reads

$$\begin{aligned} \Delta P_{AB_f}^j(t_i, t_{i+1}) &= P_{AB_f}^j(t_{i+1}) - P_{AB_f}^j(t_i) \\ &= \Delta \rho_{AB_f}^j(\alpha_i, \zeta_i, \alpha_{i+1}, \zeta_{i+1}) \\ &\quad + CPV_A^j(\alpha_{i+1}, \zeta_{i+1}) - CPV_A^j(\alpha_i, \zeta_i) \\ &\quad + \Delta \epsilon_{AB_f}(\alpha_i, \zeta_i, \alpha_{i+1}, \zeta_{i+1}). \end{aligned} \tag{10}$$

2.4 Functional model and estimation of CPV

The functional system for the Gauss–Markov model is derived from Eq. (3) by considering that the absolute value of the spherical expansion A_0^0 is not estimable. The design matrix per each observed satellite j reads

$$\bar{\mathbf{A}}^j = \left[\begin{array}{c} \Delta C_{n=1, \dots, n_{\max}}^{m=1, \dots, m_{\max}} \left| \Delta S_{n=1, \dots, n_{\max}}^{m=1, \dots, m_{\max}} \right| \mathbf{B} \end{array} \right], \tag{11}$$

with n_{\max} and m_{\max} being the maximum expansion of the SHs. If more sophisticated models for the time-differenced differential receiver clock correction are needed, \mathbf{B} is the corresponding submatrix. Depending on the receiver clock correction behaviour, different models could be applied here, e.g. polynomial clock models, frequency depending receiver clock modelling or similar approaches. For the computation of all presented CPV, we considered a differential receiver clock correction for every epoch (Kersten and Schön 2010).

As unknown parameters, the spherical harmonic coefficients A_n^m and B_n^m are estimated. Since the antenna under test is rotated and tilted, the corresponding zenith distances ζ and azimuth α angles of the line-of-sight expressed in the antenna body frame must be provided to compute the elements of $\bar{\mathbf{A}}^j$. For this transformation, the rotation angles from the robot are introduced as known values.

Generally, the maximum SH expansion for the antenna calibration is based on empirical values. It is a compromise between modelling the elevation and azimuthal variations as accurate as possible without introducing an over-parametrisation. The balance for an optimal SH expansion at IfE has been found to $SH(n, m) = SH(8, 5)$ by several empirical evaluations. For the expansion of $SH(8, 5)$, a number of 68 unknowns plus one degree of freedom (absolute value) have to be estimated. The normal equation matrices are stacked, continuously for the complete amount of epoch differences and satellites j ,

$$\left(\sum_j \bar{\mathbf{A}}^{jT} \mathbf{P}^j \bar{\mathbf{A}}^j \right) \hat{\mathbf{x}} = \sum_j \bar{\mathbf{A}}^{jT} \mathbf{P}^j \mathbf{l}^j \tag{12}$$

with the weight matrix \mathbf{P}^j and the observation vector \mathbf{l}^j filled with time-differenced RRSd for satellite j . Here, we used an identical weighting, i.e. $\mathbf{P} \equiv \mathbf{I}$. Details on the mathe-

mathematical correlations yielding a Toeplitz structure and other weighting models can be found in Kersten and Schön (2010) and Kersten (2014). The content of the observation vector is described in Sect. 2.3. Finally, the unknown SH coefficients collected in $\hat{\mathbf{x}}$ are estimated using least-squares approach,

$$\hat{\mathbf{x}} = \left(\sum_j \bar{\mathbf{A}}^{jT} \mathbf{P}^j \bar{\mathbf{A}}^j \right)^{-1} \sum_j \bar{\mathbf{A}}^{jT} \mathbf{P}^j \mathbf{l}^j. \quad (13)$$

Corresponding residuals \mathbf{v} of the observations are determined by sequentially reprocessing all design matrices $\bar{\mathbf{A}}^j$ applying the final unknown vector $\hat{\mathbf{x}}$ for all time-differenced RRSD ΔP_{AB}^j like

$$\mathbf{v} = \bar{\mathbf{A}}\hat{\mathbf{x}} - \mathbf{l}. \quad (14)$$

2.5 Operational concept of CPV estimation

The operational concept is aligned to the absolute antenna calibration concept for carrier phases, developed in Hannover in joint research projects between IfE and Geo++[®] (Wübbena et al. 1996, 2000, Seeber et al. 1997a; Böder et al. 2001; Seeber and Böder 2002).

For the CPV calibration at IfE, GNSS data are captured with Javad TRE_G3T receivers connected to a common external clock (Rubidium Frequency Standard FS725, Allan dev. of $\sigma_y = 2 \cdot 10^{-11}$). The calibration unit is a Power Cube[®] robot with 5 degrees of freedom (DOF). The rotations and tilts of the calibration unit (robot) are recorded in parallel for post-processing. A precise robot motion model is available with parameters derived from calibrations with a laser tracker (Kersten and Schön 2012). The precise robot model is introduced in a post-processing approach to estimate the SH coefficients for the CPV determination with the standard approach of degree and order SH(8, 5) using an inhouse coded IfE GNSS MATLAB Toolbox. A minimum negative elevation mask of -5° is used to stabilise the estimation of SHs at the horizon. Resulting CPV are obtained by a SH synthesis (cf. Sect. 2.2).

2.6 Exchange formats for CPV

The grid values resulting from Sect. 2.5 are stored with an interval of $5^\circ \times 5^\circ$ in an ASCII format that is based on the well-defined international Antenna Exchange Format [ANTEX, (Rothacher and Schmid 2010)]. Since the ANTEX format only supports possibilities to store and distribute PCC for relevant satellite and receiver antennas, the authors applied some refinements to store CPV, too. Therefore, the three-digit character string, which indicates the start and the end of a GNSS frequency-dependent PCC block, is replaced by a four-digit character string as already used in

RINEX 3.02 format (Gurtner and Estey 2013) as an observation code to indicate the GNSS system, the observation type, the corresponding band/frequency and the attribute for the tracking mode or channel, respectively. By this modification, the consistency of the ANTEX format is kept and it is furthermore possible, to store both, carrier and code phase-related satellite and receiver antenna correction values in one single file. Advantages as well as disadvantages of different kinds of format proposals to provide consistent sets of CPV and PCC are discussed in detail by Kersten (2014).

In addition to our marginal modifications in the ANTEX format, the company Geo++[®] provides a second format, namely ANT (Menge and Schmitz 2001), to exchange satellite- and antenna-related correction values. Even though it is possible to store with the ANT format carrier and code phase correction values, it is not possible to provide both types together in a kind of unique file with combined entities. Details on the differences and the conventions between ANTEX and ANT formats are discussed in detail by Menge and Schmitz (2001).

First experimental CPV patterns will be made available by the authors for evaluation and test purposes only.

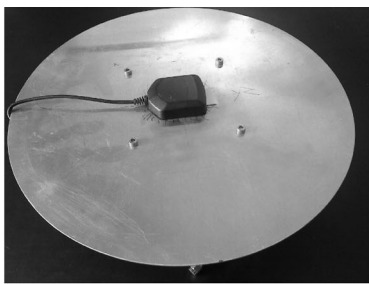
3 Discussion of obtained CPV

3.1 General remarks

The magnitudes of CPV patterns are strongly depending on the GNSS antenna design. Since the antenna design is a compromise between size, weight, gain and field of application, the properties and quality will vary. Roughly, a separation into three groups of GNSS antenna types depending on the application is possible:

- Group I** reference station antennas for multi-frequency, multi-constellation purposed (broad bandwidth), optimal reception of the GNSS code and carrier phase (heavy, stationary, expensive, elevation-dependent PCC and CPV patterns but with very small magnitudes in azimuth),
- Group II** antennas for high-quality, multi-frequency navigation approaches [light weighted, small scaled and in parts suitable for tasks where technical requirements like RTCA (2006)] have to meet,
- Group III** single-frequency antennas (narrow bandwidth antennas) that are used for simple navigation and timing.

Results presented in Figs. 2, 3 and 4 were determined as individual calibrations. For each calibration, two sets were combined with each consisting of approximate 20,000 observations. The repeatability of the individual calibrations is in



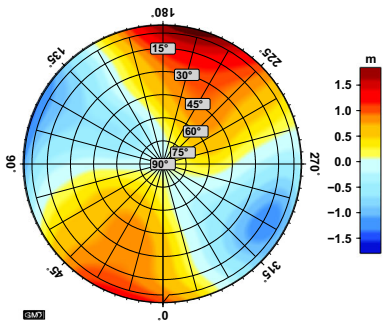
(a) μ blox ANN_MS_GP



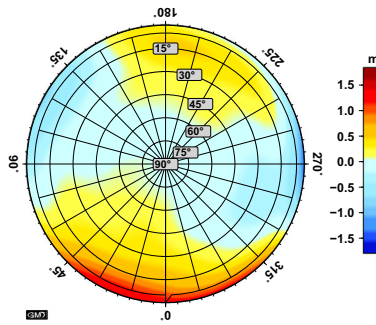
(b) Ashtech Marine



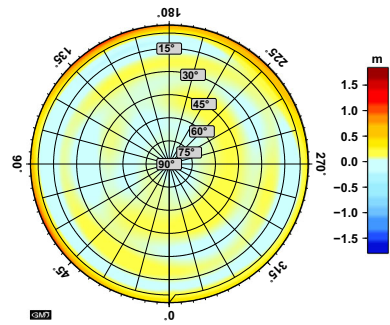
(c) Javad RegAnt_DD_E



(d) μ blox ANN_MS_GP



(e) Ashtech Marine



(f) Javad RegAnt_DD_E



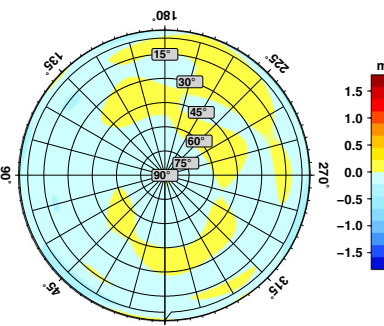
(g) NAX3G+C



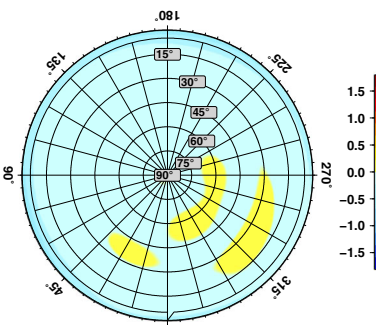
(h) Leica AX1202GG



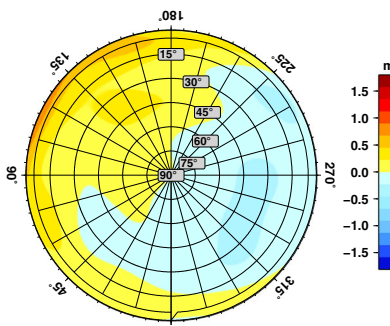
(i) Novatel NOV512+GP



(j) NAX3G+C



(k) Leica AX1202GG



(l) Novatel NOV512+GP

Fig. 2 Estimated CPV for GPS C/A code phase for several receiver antennas of group II and group III. Pronounced magnitudes are detectable for a small-scaled, single-frequency navigation antenna (a,

d), a medium CPV pattern for nautical GPS antenna (b, e), and very small deviations for an encapsulated choke ring antenna (c, f). All CPV are referred to the ARP

the range of up to 0.05 m for the elevations range of 90° down to 15°. At lower elevations, the repeatability is challenging and can have deviations of more than 0.15 m. These findings are in agreement with several sources in electro-technical

literature, e.g. Dong et al. (2006) and Rao et al. (2013). Obtained results are comparable with findings of other groups (Wübbena et al. 2008). Our study covers individual samples



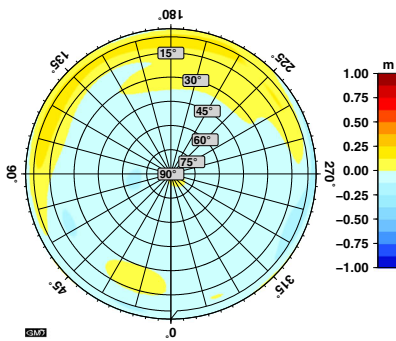
(a) Leica AR25.R3 LEIT



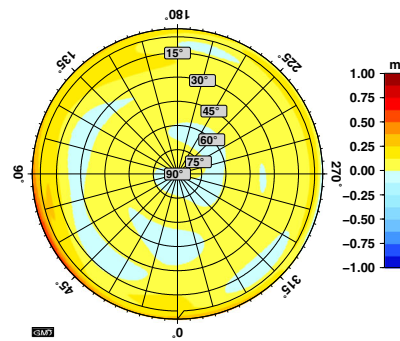
(b) Trimble Zephyr Geodetic



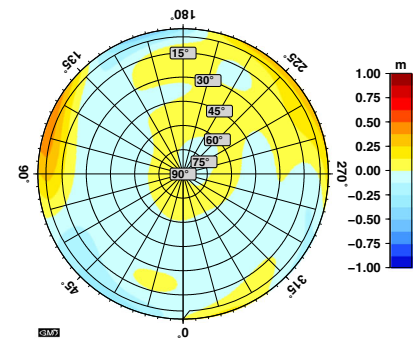
(c) Trimble TRM59900.00



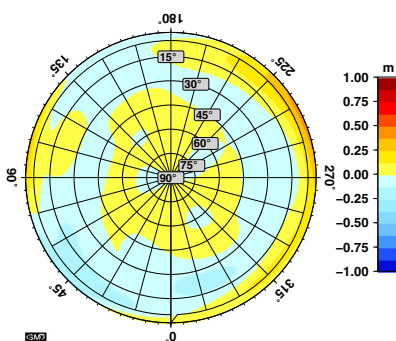
(d) GPS P1 CPV



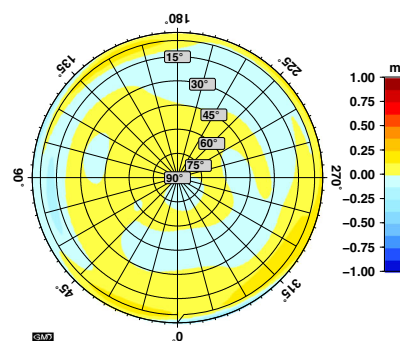
(e) GPS P1 CPV



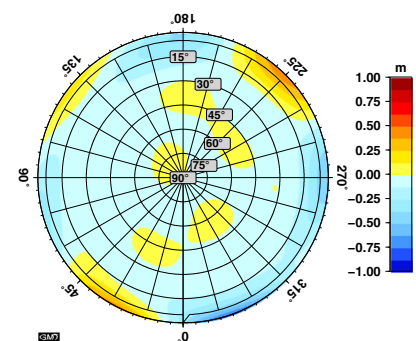
(f) GPS P1 CPV



(g) GPS P2 CPV



(h) GPS P2 CPV



(i) GPS P2 CPV

Fig. 3 Estimated CPV for GPS P1 and P2 code phase for several geodetic high precision GPS/GNSS antennas (group I). Magnitudes can be identified with an amount of up to 0.4 m. In contrast to C/A CPV a

homogeneous hemispherical distribution is obtained. Furthermore, signal dependency of the CPV were identified for all kinds of analysed GPS/GNSS antennas

of different GNSS antenna types. Further analyses should focus on

1. determining type mean values for CPV to assess the stability of the CPV pattern in different product series,
2. evaluating limits of the CPV determination as well as
3. improving the CPV determination at low elevations.

CPV are identified during our studies to be antenna-related characteristics. They are independent of time and location of calibration. This could be verified by different orientations of the antenna in the calibration process. Thus, a changed horizontal orientation of the antenna in the calibration pro-

cess yields to a rotation of the determined CPV pattern, as expected.

3.2 CPV of GPS C/A signal

Results of CPV for GPS C/A for several antennas are summarised in Fig. 2. Contrary to the definition of PCC, the obtained CPV are referred directly to the ARP with a code phase centre offset equal to zero ($CPO \equiv 0$). However, the determined corrections include the complete information that could be transformed to any arbitrary CPO as shown in Schön and Kersten (2013). Please remember that comparisons of CPV (as well as PCC) by individual polar representation (see

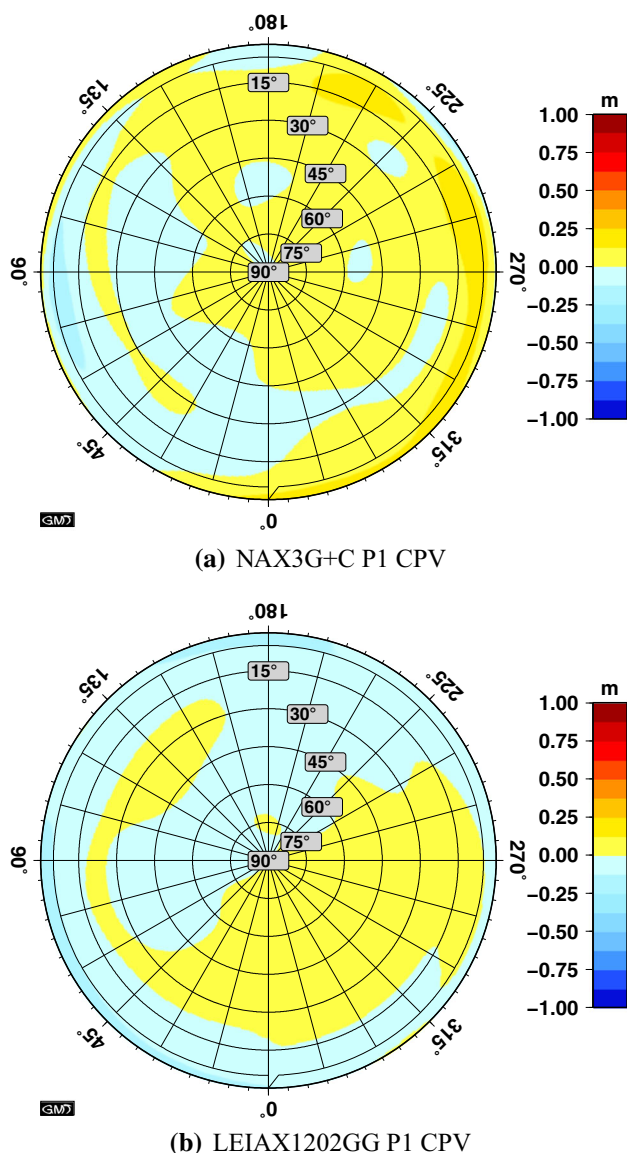


Fig. 4 Estimated CPV for antennas of group II, **a** geodetic multi-frequency antenna (navXperience 3G+C) with one-layer technology (Popugaev and Wansch 2009) and **b** Leica AX1202GG rover antenna with pinwheel technology (Kunysz 2000)

subfigures in Fig. 2) are only meaningful if they are referred to a common reference point, here the ARP.

Considering the distribution of the variations, a clear dependency with azimuth and elevation is visible. Furthermore, the magnitudes differ for each individual receiver antenna or receiver antenna design, respectively.

The most pronounced values are detected for an antenna of group III (cf. Fig. 2d), where deviation of up to 1.8 m has been obtained and verified. The variations are closely related to the design (feeding configuration) of the micro-patch elements (Dong et al. 2006).

Although the variations are smaller and occur at low elevations, the Ashtech antenna (group II, cf. Fig. 2e) shows also variations of up to 0.6 m, distributed non-symmetrically over the antennas hemisphere. Definitely smaller CPV were obtained for antennas of group I [encapsulated choke ring antenna (Fillipov et al. 1998)] which are typical geodetic antennas in majority, as shown in Fig. 2j–l. There, the variations are well below 0.3 m and therefore below the code noise of most of the current code signals.

Referring to Fig. 2l, a very dominant shift of the complete pattern from +0.3 m in the north-west to −0.3 m in the east-south is obtained. Such characteristics in antenna patterns are explainable by an existence of a mean code phase offset, mainly in the horizontal component. This effect has to be analysed in detail in further studies.

3.3 CPV of GPS P1 and P2 signal

CPV were also determined for several antennas of group I for the P code signal. The existence of CPV for the P signal could be identified. It has been elaborated (cf. Fig. 3) that the obtained CPV differ for each antenna depending on the signal and frequency (Kersten 2014). Furthermore, for the same antenna, CPV are different for each individual signal and frequency and above the noise level of the CPV determination.

For antennas of group I, Fig. 3 shows exemplarily that the effect of CPV is in the range of 0.3–0.4 m and therefore quite small compared to the assumed overall noise of the code phase observation. At lower elevations (below 15°), currently the CPV have to be compared and discussed carefully.

The Trimble Zephyr antenna, as shown in Fig. 3e, h, has a significant offset for the CPV on P1 that is translated by a slight slope in the CPV pattern. The overall offset is in the range of 0.25 m (maximal amplitudes) and smaller than the obtained values for the CPV on P2. Nevertheless, CPV on P2 have a magnitude of 0.15 m and are additionally smaller than the values obtained for CPV P1.

The estimated CPV for a 2D (Trimble TRM59900.00 NONE) and a 3D (Leica AR25.R3 LEIT) choke ring antenna (Tranquilla and Colpitts 1989; Tranquilla et al. 1994; Kunysz 2003) provide very homogeneous patterns with magnitudes below 0.15 m. They are obtained from four sets of individual calibrations and similar antenna types (cf. Fig. 3d, f, g, i). Furthermore, similar magnitudes are determined for multi-GNSS pinwheel antennas (Kunysz 2000; Popugaev and Wansch 2009). Figure 4 summarises exemplary the results of two small-scaled geodetic GNSS antennas with a broad bandwidth and multi-frequency properties. The comparable CPV characteristics for pinwheel antennas wrt. Two-dimensional and 3D choke ring antennas are interesting and show the quality of different antenna designs.

These results are derived from a small amount of individually analysed geodetic and non-geodetic antennas tested along with our study. They are in good agreement with the findings of Wübbena et al. (2008). This group analysed several antennas of group I with the same robot system, but with a different estimation approach. They also found similar small CPV for GNSS reference station antennas on the GPS P1 and P2 signal.

4 Validation of CPV

4.1 Experimental set-up

Since different error sources are supposed to be suppressed during the calibration process, it seems worth to test these assumptions by dedicated experiments. In parallel, these experiments underline that CPV are antenna-specific properties and individual for each antenna. In addition, it is mandatory to understand how CPV influence the estimation of geodetic parameters, e.g. coordinates or time. For answering this question and validate the findings of Sect. 3, experiments were performed on the laboratory roof top network at IfE, cf. Fig. 7a.

On a short baseline, two Javad TRE_G3T receivers of the same kind were connected to a μ blox antenna (cf. Fig. 2a) at the one end and to a Leica AR25.R3 reference station antenna (Fig. 3a) at the other end. Data were recorded for three days (DOY 223 - 225, 2012) under very similar weather conditions. In addition, the orientation of the μ blox antenna was changed by $+240^\circ$ between the days DOY 223 and DOY 225, 2012. The data were recorded with 1-second sampling interval and with a cut-off angle of zero degree. No code smoothing was applied. Both receivers were connected to a common external frequency standard (Rubidium Frequency Standard FS725). Thanks to its frequency stability, RRSD can be formed for the analysis. The coordinates of the pillars were known with high accuracy.

4.2 Impact of GPS C/A CPV on the observation domain

Figure 5 shows the observed-minus-computed (OMC) values of RRSD for two exemplary satellites, PRN4 at medium elevation and PRN20 at high elevation. Thanks to the common clock short baseline set-up and the precisely known coordinates of the baseline endpoints, almost all systematic effects will cancel and flat OMC time series are expected. However, significant and systematic deviations from the expected constant value are obtained. They are explainable by considering the CPV of both antennas correctly. The corresponding CPV correction for the short baseline is indicated as solid red line in Fig. 5.

Due to the sidereal repetition of the GPS constellation, in general the same but time-shifted RRSD deviations would be expected for consecutive days like DOY 223-225 for the sample satellites PRN4 and PRN20 in the case that the orientation of none of the receiver antennas is changed. As the expected behaviour of the RRSD could be detected between DOY 223 and DOY 224, significant differences between the RRSD of DOY 225 and DOY 223 are obvious in Fig. 5 for the sample satellites PRN4 and PRN20. This is explainable by the impact of the pronounced CPV pattern of the used patch antenna. Since we intentionally rotated the patch antenna between both days by $+240^\circ$, the changed CPV dominates the behaviour of the time series (cf. Fig. 5c, d). This can be illustrated very well by the interpolated corrections on the RRSD derived from the antenna-specific CPV and shown as solid line in Fig. 5.

Considering the CPV corrections at this experiment improves the RRSD to zero mean. Thus, it could be shown that CPV are antenna-dependent and the pattern is not created by multipath.

4.3 Impact of GPS C/A CPV on the position domain

Improvements for single point positioning (SPP) solutions (Seeber 2003) by considering CPV are achievable, as long as the antennas used for positioning have a pronounced CPV pattern above the overall code noise level. In order to quantify the impact, epochwise positions were computed for three days with identical and elevation-dependent weighting. The patch antenna depicted in Fig. 2d was used. The reference coordinates of the pillar were precisely known. Between DOY 224 and DOY 225, the patch antenna was horizontally rotated by $+240^\circ$. The position residuals of the SPP runs wrt. reference coordinate are collected in Table 2.

Referring to Table 2, an improvement of the accuracy of the SPP solution is obtained when CPV corrections were considered correctly. The horizontal components are improved in RMS by up to 0.2 m (10%) and the up component by up to 0.3 m (15%).

The cumulative distributions of position residuals wrt. the reference coordinates are shown in Fig. 6. The horizontal components can be reduced to the same level for all three days by applying the CPV corrections (cf. Fig. 6a, b). The cumulative distributions for the uncorrected data show a scatter between the different days. Since the residuals contain noise and further remaining systematics like unmodelled ionospheric refraction effects with changing impact from day to day, a further interpretation or clear attribution of different CPV is not obvious. Overall, the repeatability of the position residuals in all three directions is much more homogeneous after applying the CPV corrections.

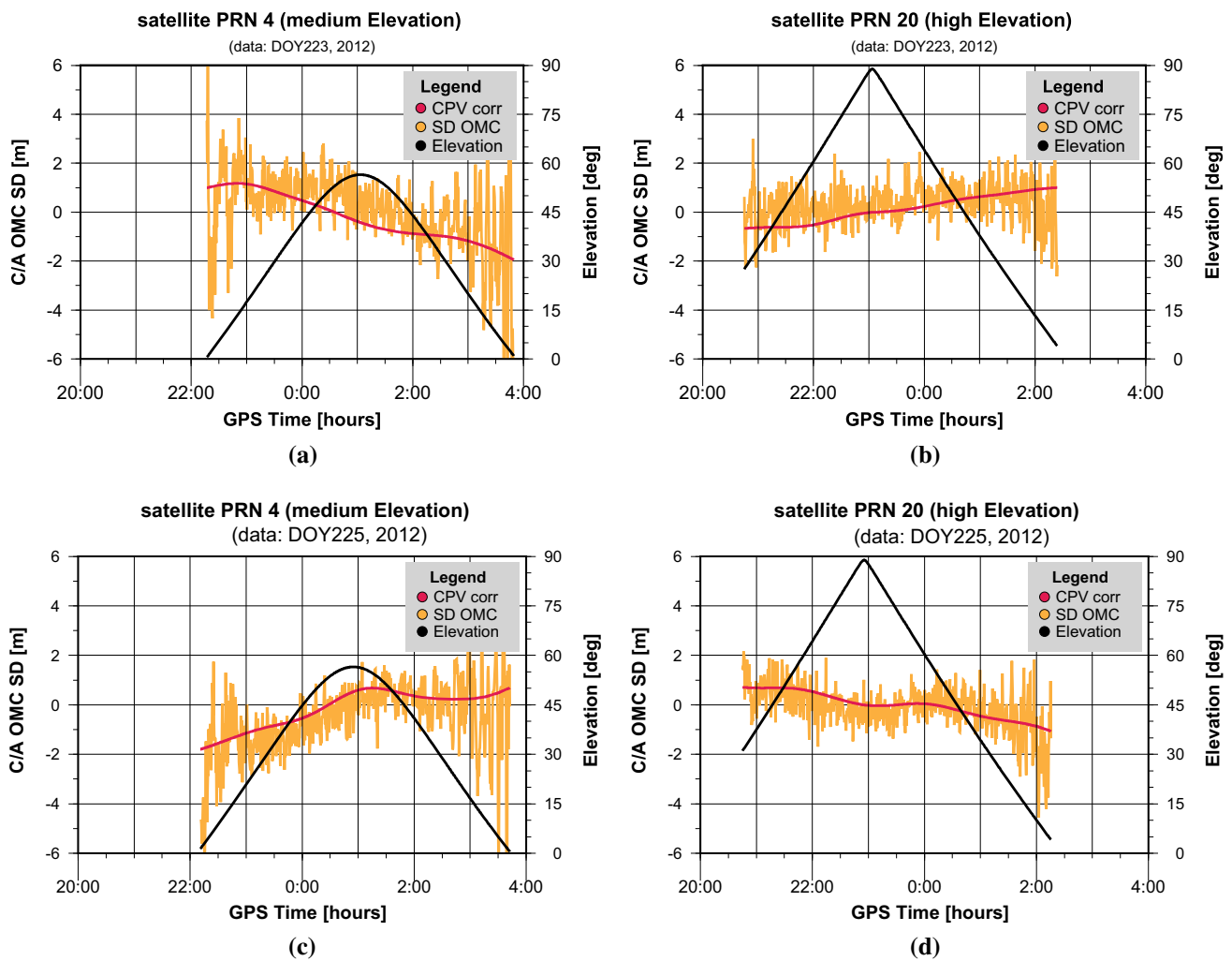


Fig. 5 Observed-minus-computed (OMC) values of receiver-to-receiver single differences (RRSD) of a short baseline (7 m) in a common clock set-up. The graphs show the impact of CPV on the observation domain. Sidereal repetition with changed satellite geometry and

antenna orientation is exemplarily shown for two GPS satellites. The antenna orientation of one station is changed between DOY 223 and DOY 225 by +240° to illustrate the antenna-specific property of CPV

Table 2 RMS of position residual time series of SPP runs w.r.t precise reference coordinates with (y) and without (n) considering corrections for CPV

DOY-CPV	RMS SPP Solution					
	Identical weighting			Elevation weighting		
	North [m]	East [m]	Up [m]	North [m]	East [m]	Up [m]
223-n	0.875	0.639	1.798	1.113	0.686	1.891
223-y	0.794	0.572	1.707	0.900	0.645	1.695
0°	+9%	+10%	+5%	+19%	+6%	+10%
224-n	0.913	0.648	1.749	0.870	0.649	1.920
224-y	0.738	0.569	1.551	0.874	0.655	1.679
0°	+19%	+12%	+11%	+0%	+0%	+13%
225-n	1.097	0.552	2.038	1.000	0.590	2.122
225-y	0.800	0.494	1.680	0.904	0.574	1.814
240°	+27%	+11%	+18%	+10%	+3%	+15%

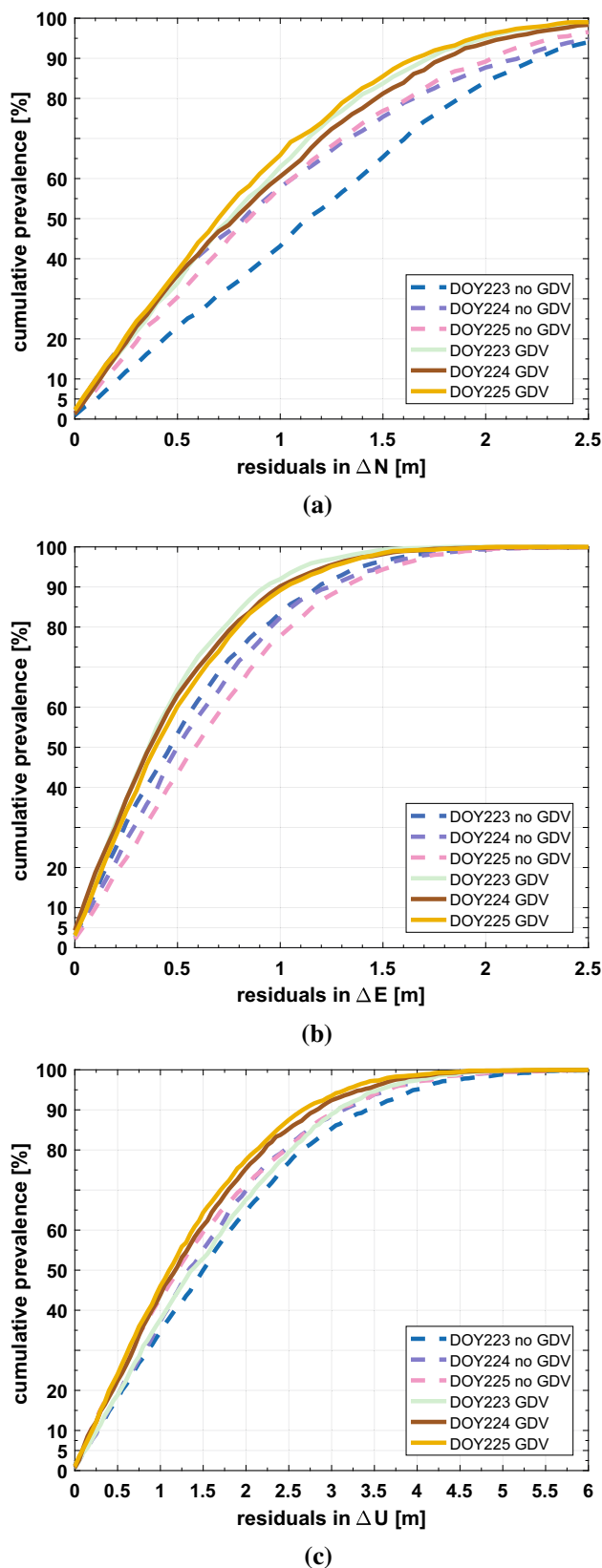


Fig. 6 Improvements in cumulative percentage of the residuals obtained from single point positioning (SPP) using identical weighting, **a**, **b** horizontal components, **c** height component

4.4 Impact of GPS CPV on the time domain

As a side remark, it should be noted that in several studies we evaluated the impact of CPV on precise time and frequency transfer. The current impact is below the process noise for the code only (Kersten and Schön 2011) and for the code and carrier phase combined approaches (Kersten et al. 2012). However, for modern low noise GNSS code signals like MBOC or AltBOC modulation significant patterns could potentially influence time and frequency transfer in future.

5 Impact of GPS P1/P2 CPV on the ambiguity resolution

5.1 Ambiguity resolution with Melbourne–Wübbena linear combination

Based on studies from Hatch (1982) about the synergy of carrier and code phase observations, Melbourne (1985) and Wübbena (1985) presented independently from each other a robust method to determine carrier phase ambiguities by combining carrier and code phase observations on two frequencies, the Melbourne–Wübbena linear combination (MW-LC) (Seeber 2003),

$$\begin{aligned}\Phi_{A_w}^j &= \frac{f_1}{f_1 - f_2} \Phi_{A_1}^j - \frac{f_2}{f_1 - f_2} \Phi_{A_2}^j \\ &= \bar{\rho}_A^j + \frac{f_1}{f_2} I_1 + \lambda_w N_{w,A}^j + d_A - d^j\end{aligned}\quad (15)$$

$$\begin{aligned}P_{A_w}^j &= \frac{f_1}{f_1 + f_2} P_{A_1}^j + \frac{f_2}{f_1 + f_2} P_{A_2}^j \\ &= \bar{\rho}_A^j + \frac{f_1}{f_2} I_1\end{aligned}\quad (16)$$

with the frequency f , the widelane linear combination $\Phi_{A_w}^j$ of the L1 and L2 carrier phase observations $\Phi_{A_1}^j, \Phi_{A_2}^j$, respectively, from station A to a specific satellite j and the receiver- and satellite-related signal biases d_A and d^j . The widelane ambiguity is denoted by $N_{w,A}^j$ with its respective wavelength $\lambda_w = 0.86$ m. The ionospheric effect on L1 is I_1 . The non-dispersive parts (i.e. geometry) are summarised in $\bar{\rho}_A^j$. The code observations are denoted in analogy by $P_{A_1}^j$ and $P_{A_2}^j$.

The MW-LC is used to eliminate the geometry and ionospheric delay by

$$MW_A^j = \Phi_{A_w}^j - P_{A_w}^j = \lambda_w N_{w,A}^j.\quad (17)$$

This linear combination is especially relevant for inter-continental and very long baselines as it is independent of ionosphere and geometry. However, observations on both frequencies and low noise code observations are necessary. The

signal biases d_A and d^j destroy the pure integer nature, but can be eliminated by double differences (DD) between two stations A, B and satellites j, k , modelled by the widelane DD ambiguities,

$$N_{w,AB}^{jk} = \lambda_w(N_{1,AB}^{jk} - N_{2,AB}^{jk}) = \Phi_{w,AB}^{jk} - P_{w,AB}^{jk} \quad (18)$$

Equation (17) indicates that the code phases on both frequencies are combined with each other, so that the impact of CPV is amplified and possibly reaches magnitudes affecting the ambiguity resolution (cf. Eq. 18). An experiment was carried out to analyse the impact of the individual antenna properties on the ambiguity resolution.

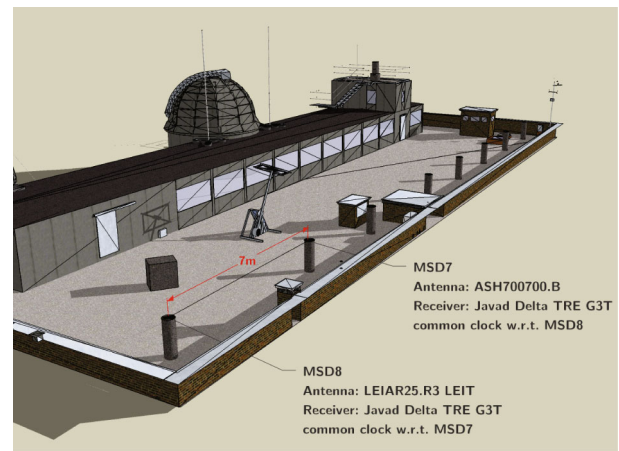
5.2 Experimental set-up

Two antennas with different CPV pattern were installed at the end points of a short baseline located at the laboratory network of IfE, to analyse the impact of CPV on the ambiguity resolution. The set-up of the experiment is depicted in Fig. 7. On pillar MSD7, an Ashtech Marine Antenna (Ashtech ASH700700B, cf. Fig. 2b) with significant CPV is installed together with a Javad Delta TRE_G3T (serial number 081) receiver. On pillar MSD8, a 3D choke ring antenna (Leica AR25.R3, cf. Fig. 3a) with minimal CPV is mounted in combination with the same receiver type (serial number 082). The coordinates of both baseline endpoints are known with high precision since as they are part of the IfE laboratory network. They serve as ground truth so that the impact of CPV on the baseline components can be studied.

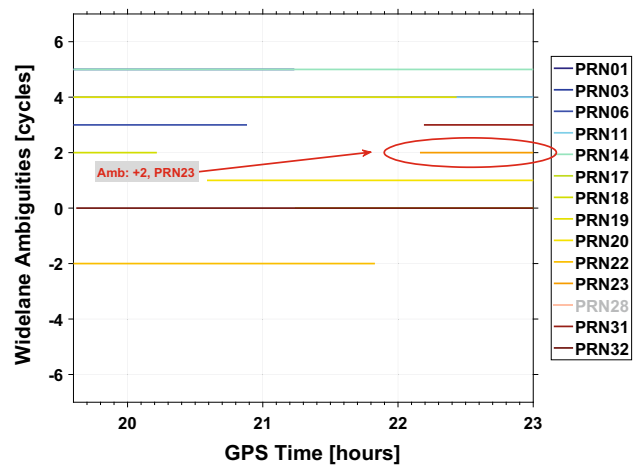
5.3 Results

In Fig. 7b, c, the widelane ambiguities of double differences of Melbourne–Wübbena linear combinations (DD MW-LC) are depicted for an exemplary time window. The DD MW-LC are not shown here. In addition to the characteristic noise level of ± 0.5 to ± 0.7 m, drifts are superimposed created by the CPV. The impact exceeds the magnitude of the MW wavelength of $\lambda_w = 0.86$ m and can corrupt the correct MW-LC ambiguity resolution by up to a full widelane cycle. This is shown by Fig. 7a, c. Considering the CPV corrections for the used antenna models yields to a different widelane ambiguity as indicated by Fig. 7c. There, the widelane ambiguity of the satellite PRN23 changes from +2 widelane cycle (no CPV applied) to +1 widelane cycles (CPV applied).

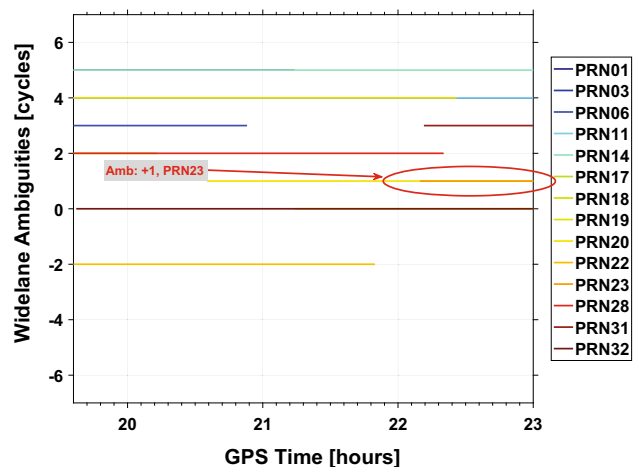
Already one incorrectly resolved widelane ambiguity is enough to introduce jumps and drifts in the coordinate estimates or destroys the solution completely. This can be seen directly for a widelane coordinate solution shown for illustration purpose here. Typically, widelane coordinates are not used since they are very noisy as depicted in Fig. 8. But the effects of erroneous widelane ambiguity solution are clearly



(a) Laboratory Network of IfE



(b) Widelane Ambiguities (no CPV applied)



(c) Widelane Ambiguities (CPV applied)

Fig. 7 Experiment to analyse the impact of antenna properties on the ambiguity resolution, a set-up at laboratory network of IfE, b, c widelane phase ambiguities of double differences (DD) of Melbourne–Wübbena linear combination (MW-LC). For satellite PRN23, a widelane cycle jump (from +2 to +1 widelane cycle) is introduced that can be repaired by applying CPV

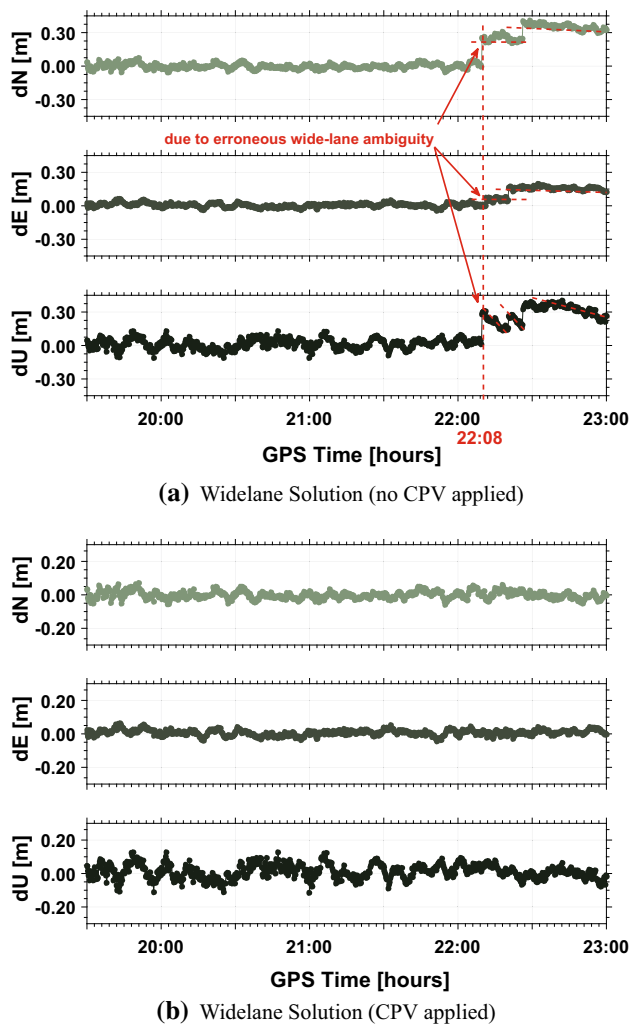


Fig. 8 Impact of the antennas response exemplary shown for the widelane coordinate solution, **a** derivations of the coordinate estimates for all components due to wrong resolved widelane ambiguities, **b** considering CPV on the widelane resolves the ambiguities correctly

visible (cf. Fig. 8a). It was identified that the starting point of jumps and drifts corresponds well to the start of a wrongly fixed widelane ambiguity. Further jumps are introduced by subsequent changes of the number and configuration of visible satellites. Considering the CPV corrections during the widelane processing corrects the widelane ambiguity and yields zero mean coordinate residuals, (cf. Fig. 8b).

After solving the widelane ambiguities, L1 ambiguities are obtained. Hence, one wrong widelane ambiguity will introduce directly an erroneous L1 ambiguity with a magnitude of four, as depicted for the satellite PRN23 in Fig. 9a, b. Consequently, the epochwise L1 coordinate estimates show jumps and drifts when wrong ambiguities appear as indicated by Fig. 9c. Considering the CPV as an antenna-related effect helps solving the widelane and corresponding L1 ambiguity correctly and improves the kinematic L1 position residuals

(cf. Fig. 9d). The resulting position residuals have zero mean with a typical scatter of ± 0.01 m maximum deviation in the horizontal and ± 0.03 m in the up component, respectively.

The improvement and success of applying the corresponding CPV corrections depend strongly on the processing scheme and can be summarised by mainly the following two conditions:

- A smoothing of the code by carrier phase observations can have additional negative impact on the MW-LC, since the CPV effect is a long-term trend. Therefore, the effect of CPV can be reduced by optimal combination of filtering and average time.
- Depending on the time window of data recording and of the magnitudes of antenna CPV, an elevation weighting can reduce the impact of CPV on short observation time spans at least at low elevations, since they are appropriately down-weighted.

Consequently, the impact of CPV can be significantly reduced by selecting adequate processing schemes.

6 Conclusions

This paper describes the methodology to estimate code phase variations (CPV) of GNSS receiver antenna based on the Hannover concept of absolute antenna calibration. Selected calibration results are presented and discussed. The impact of CPV on positioning is investigated using the example of single point positioning and ambiguity resolution.

The CPV magnitudes depend on the antennas design as well as on the signal modulation and frequency. The obtained CPV are elevation and azimuth dependent. For antennas of group I (geodetic multi-frequency and multi-constellation antennas), the pattern is very homogeneous and below the code noise level with magnitudes below 0.30 m. Similar results were obtained for some antennas of group II (rover or RTK antennas). However, antennas of group II/III (navigation antennas or older designs) like Ashtech Marine antenna show significant CPV above the code noise level with magnitudes of up to 0.6 m. The most pronounced CPV patterns were determined for a small-scaled GPS micro-patch antenna. There, large magnitudes of up to 1.8 m for GPS C/A could be identified. This variability should be kept in mind when precise coordinates are to be determined with small-scaled, low-cost as well as low-weight antennas.

To start a discussion of the relevance of CPV (or group delay variations GDV) in the GNSS satellite and receiver antenna community and for test and evaluation purposes only, we make experimental CPV patterns available by request.

In the observation domain, we showed that CPV introduce significant and reproducible systematic effects. Calibrating

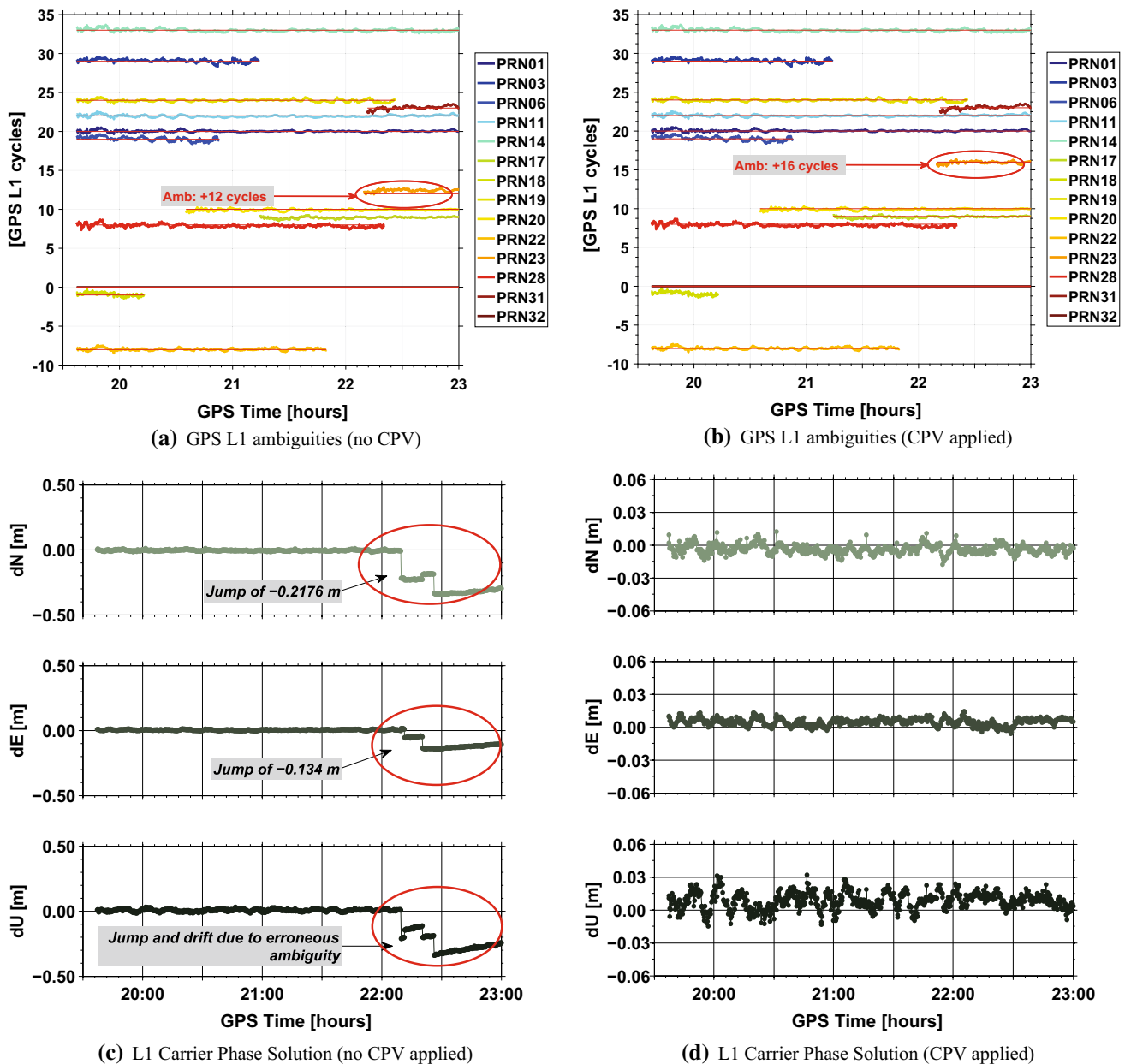


Fig. 9 Impact of CPV on the MW-LC ambiguity resolution, **a, b** L1 ambiguities are resolved differently due to wrong widelane ambiguity, **c, d** jumps and drifts in the L1 carrier phase solution can be avoided using CPV correction

and applying additional corrections will not remove the overall noise, but the systematic signature of CPV from the observations. Using dedicated experiments with rotated antennas, we showed that a pronounced CPV pattern dominates the observation time series, and thus, the effect is separable from possible multipath.

Position residuals wrt. reference coordinates could be reduced by considering CPV for small-scaled GPS patch antennas. This is possible as long as the CPV are above the code noise level. Furthermore, it was shown that CPV can also influence the ambiguity resolution with the Melbourne–

Wübbena strategy yielding potentially large deviations (up to dm level) in the coordinates of the final L1 solution.

In future, improved system designs and upgraded signals structures like the MBOC (multiple binary offset carrier) and AltBOC (alternative BOC modulation) signals will decrease the overall noise level of the code observations. Thus, considering CPV will become even more important.

Acknowledgements The authors gratefully acknowledge the funding of this research by the German Federal Ministry of Economics and Technology with the label 50 NA 0903 and 50 NA 1216. In addition,

both anonymous reviewers are thanked for their valuable and useful comments on the manuscript.

References

- Aerts W (2011) Comparison of UniBonn and Geo++[®] calibration for LEIAR25.R3 antenna 09300021. Technical report, Royal Observatory of Belgium
- Aerts W, Baire Q, Bilich A, Bruyninx C, Legrand J (2013) On the error sources in absolute individual antenna calibrations. In: Geophysical research abstracts, EGU2013-6113, vol 15. EGU General Assembly 2013, Vienna
- Aerts W, Moore M (2013) Comparison of UniBonn and IGS08 antenna type means. In: White paper, International GNSS Service—Antenna Working Group IGS-AWG. EMail: IGS-AWG-393. ftp://ftp.sirgas.org/pub/igs/AntennaComparisons-Merged_final.pdf
- Altamimi Z, Rebischung P, Métivier L, Collilieux X (2016) ITRF2014: a new release of the International Terrestrial Reference Frame modelling nonlinear station motions. *J Geophys Res.* doi:10.1002/2016JB013098
- Böder V, Menge F, Seeber G, Wübbena G, Schmitz M (2001) How to deal with station dependent errors, new developments of the absolute field calibration of PCV and phase-multipath with a precise robot. In: Proceedings of the 14th international technical meeting of the satellite division of the institute of navigation (ION GPS 2001), September 11–14, Salt Lake City, UT, USA. Institute of Navigation (ION), pp 2166–2176
- Defraigne P, Petit G (2003) Time transfer to TAI using geodetic receivers. *Metrologia* 40(4):184–188. doi:10.1088/0026-1394/40/4/307
- Dong W, Jackson DR, Williams JT, Basilio LI (2006) Phase and group delays for circularly-polarized microstrip antennas. In: Proceedings of antennas and propagation society international symposium, July 9–14, Albuquerque, NM, USA. IEEE, pp 1537–1540. doi:10.1109/APS.2006.1710847
- Engheta N, Ziolkowski RW (eds) (2006) *Metamaterials: physics and engineering explorations*. Wiley-IEEE Press, Piscataway
- Fillipov V, Tatarnikov D, Ashjaee J, Astakhov A, Sutiagin I (1998) The first dual depth frequency choke ring antenna. In: Proceedings of the 11th international technical meeting of the satellite division of the institute of navigation (ION GPS 1998), September 15–18, Nashville, TN, USA Institute of Navigation (ION), pp 1035–1040
- Geiger A (1988) Modelling of phase centre variation and its influence on GPS-positioning. In: Groten E, Strauss R (eds) *GPS-techniques applied to geodesy and surveying*, Lecture notes in earth sciences, vol 19 of proceedings of the international GPS-workshop Darmstadt, April 10–13, 1988. Springer, Berlin, pp 210–222. doi:10.1007/BFb0011339
- Görres B, Campbell J, Becker M, Siems M (2006) Absolute calibration of GPS antennas: laboratory results and comparison with field and robot techniques. *GPS Solut* 10(2):136–145. doi:10.1007/s10291-005-0015-3
- Gurtner W, Estey L (2013) RINEX The receiver independent exchange format. IGS publications. <ftp://igs.org/pub/data/format/rinex302.pdf>
- Haines B, Bertiger W, Desai S, Harvey N, Sibois A, Weiss J (2012) Characterizing the GPS satellite antenna phase- and group-delay variations using data from low-earth orbiters. In: IGS Workshop 2012, University of Warmia and Mazury, Olsztyn, Poland, 23–27 July
- Hatch R (1982). The synergism of GPS code and carrier measurements. In Peat RP, (ed) *Proceedings of the third international geodetic symposium on satellite doppler positioning*, vol 2. Defense Mapping Agency and National Ocean Survey, Las Cruces, NM, USA, pp 1213–1231, 8–12 Feb
- Hobson E (1931) *The theory of spherical and ellipsoidal harmonics*. University Press, Cambridge
- Hofmann-Wellenhof B, Moritz H (2006) *Physical geodesy*. Springer, Berlin
- Huang Y, Boyle K (2008) *Antennas—from theory to practice*. Wiley, Chichester
- IGS (2016a). International GNSS Service: details and naming conventions for IGS equipment—rcvr_ant.tab. electronic. ftp://igs.org/pub/station/general/rcvr_ant.tab
- IGS (2016b). International GNSS Service: graphical receiver antenna reference point—(ARP) Definition—antenna.gra. electronic. <ftp://igs.org/pub/station/antenna.gra>
- Kaniuth K, Stuber K (2002) The impact of antenna radomes on height estimates in regional GPS networks. In: Drewes H, Dodson AH, Fortes LPS, Sánchez L, Sandoval P (eds) *International association of geodesy symposia on vertical reference systems*, vol 124. Berlin, Springer, pp 101–106
- Kaplan ED (ed) (1996) *Understanding GPS—principles and applications*. Artech House Inc, Norwood
- Kersten T (2014) Bestimmung von Codephasen-Variationen bei GNSS-Empfangsantennen und deren Einfluss auf die Positionierung, Navigation und Zeitübertragung. Ph.D. thesis, Deutsche Geodätische Kommission (DGK) bei der Bayerischen Akademie der Wissenschaften (BADW), no. 740
- Kersten T, Schön, S (2010) Towards modeling phase center variations for multi-frequency and multi-GNSS. In: 5th ESA workshop on satellite navigation technologies and european workshop on GNSS signals and signal processing (ESA Navitec), pp 1–8. doi:10.1109/NAVITEC.2010.5708040
- Kersten T, Schön S (2011) GNSS group delay variations—potential for improving GNSS based time and frequency transfer? In: Proceedings of the 43rd annual precise time and time interval (PTTI) meeting. Long Beach, CA, pp 255–270
- Kersten T, Schön S (2012) Von der Komponentenkalibrierung zur Systemanalyse: Konsistente Korrekturverfahren von Instrumentenfehlern für Multi-GNSS—Schlussbericht zum BMBF/DLR Vorhaben 50NA0903. Institut für Erdmessung, p 105
- Kersten T, Schön S, Weinbach U (2012) On the impact of group delay variations on GNSS time and frequency transfer. In: Proceedings of the 26th European frequency and time forum (EFTF), 24–26 April 2012, Gothenborg, Sweden, pp 514–521. doi:10.1109/EFTF.2012.6502435
- Kim U-S (2005) Analysis of carrier phase and group delay biases introduced by CRPA hardware. In: Proceedings of the international technical meeting of the satellite division of the institute of navigation (ION-GNSS), 13–16 Sep 2005, Long Beach, CA, USA. Institute of Navigation (ION), pp 635–642
- Kouba J (2004) Improved relativistic transformations in GPS. *GPS Solut* 8(4):170–180. doi:10.1007/s10291-004-0102-x
- Kouba J (2009) A guide to using international GNSS service (IGS) products. IGS Publications. <http://acc.igs.org/UsingIGSProductsVer21.pdf>
- Kube F, Schön S, Feuerle T (2012) GNSS-based curved landing approaches with a virtual receiver. In: Proceedings of the position location and navigation symposium (ION-PLANS), 2012 IEEE/ION, 23–26 April, SC, USA. Institute of Navigation (ION), pp 188–196
- Kunysz W (1998) Effect of antenna performance on the GPS signal accuracy. In: 11th international technical meeting of the satellite division of the institute of navigation (ION) GPS98, 15–18 Sep 1998, Nashville, TN, USA. Institute of Navigation (ION), pp 575–580
- Kunysz W (2000) High performance GPS pinwheel antenna. In: Proceedings of the 2000 international technical meeting of the satellite

- division of the institute of navigation (ION GPS 2000), 19–22 Sep, Salt lake City, Utha USA. ION
- Kunysz W (2003). A three dimensional choke ring ground plane antenna. In: Proceedings of the 16th international technical meeting of the satellite division of the institute of navigation (ION GPS/GNSS 2003), 9–12 Sep, Portland, OR, USA. Institute of Navigation (ION), pp 1883–1888
- Mader G (1999) GPS antenna calibration at the National Geodetic Survey. *GPS Solut* 3(1):50–58. doi:[10.1007/PL00012780](https://doi.org/10.1007/PL00012780)
- Mader GL, MacKay JR (1996) Calibration of GPS antennas. In: Neilan R, Scoy PV, Zumbege J (eds) Proceedings of the IGS analysis center workshop, Silver Spring, MD. JPL Publication 96-26, Jet Propulsion Laboratory, Pasadena, CA
- Melbourne, WG (1985) The case for ranging in GPS-based geodetic systems. In: Goad CC (ed) Proceedings of the first international symposium on precise positioning with the global positioning system, Rockville, MD, 15–19 Apr
- Menge F, Schmitz M (2001) Format and Geo++[®] convention for PCV antenna files. Manual. https://www.ife.uni-hannover.de/pcv_ant-format.html and http://www.geopp.com/media/docs/AOA_DM_T/format.html
- Murphy T, Geren P, Pankaskie T (2007) GPS antenna group delay variation induced errors in a GNSS based precision approach and landing systems. In: Proceedings of the 20th international technical meeting of the satellite division of the institute of navigation (ION GNSS 2007), 25–28 Sep, Fort Worth, TX, USA. Institute of Navigation (ION), pp 2974–2989
- Petrovski IG, Tsujii T (2012) Digital satellite navigation and geophysics. Cambridge University Press, Cambridge
- Popugaev A, Wansch R (2009) A novel miniaturization technique in microstrip feed network design. In: Proceedings of European conference on antennas and propagation (EuCAP), 23–27 March 2009, Berlin, Germany, pp 2309–2313
- Rao BR, Kunysz W, Fante RL, McDonalds K (2013) GPS/GNSS antennas. Artech House Publishers, Norwood
- Ray J, Senior K (2003) IGS/BIPM pilot project: GPS carrier phase for time/frequency transfer and timescale formation. *Metrologia* 40:270–288
- Ray J, Senior K (2005) Geodetic techniques for time and frequency comparisons using GPS phase and code measurements. *Metrologia* 42(4):215–232. doi:[10.1088/0026-1394/42/005](https://doi.org/10.1088/0026-1394/42/005)
- Rothacher M, Schmid R (2010) ANTEX: the antenna exchange format, Version 1.4. ftp://igs.cb.jpl.nasa.gov/igs_cb/station/general/antex14.txt
- RTCA (2006). Minimum operational performance standards for global navigation satellite system (GNSS) airborne active antenna equipment for the L1 frequency band. RTCA/DO-301 Inc. Washington DC, Issued 13 Dec 2006
- Schmid R (2013) Uncertainty of GNSS antenna phase center corrections. In: IERS workshop on Local Surveys and Co-locations, 22 May, Paris
- Schmid R (2016) Antenna Working Group technical report 2015. In: Jean Y, Dach R (eds) International GNSS service technical report 2015, pp. 141–145. doi:[10.7892/boris.80307](https://doi.org/10.7892/boris.80307)
- Schmid R, Dach R, Collilieux X, Jäggi A, Schmitz M, Dilssner F (2016) Absolute IGS antenna phase center model igs08.atx: status and potential improvements. *J Geod* 69(4):343–364. doi:[10.1007/s00190-015-0876-3](https://doi.org/10.1007/s00190-015-0876-3)
- Schmid R, Rothacher M, Thaller D, Steigenberger P (2005) Absolute phase center corrections of satellite and receiver antennas—impact on global GPS solutions and estimation of azimuthal phase center variations of the satellite antenna. *GPS Solut* 9(4):283–293. doi:[10.1007/s10291-005-0134-x](https://doi.org/10.1007/s10291-005-0134-x)
- Schön S, Kersten T (2013) On adequate comparison of antenna phase center variations. In: American Geophysical Union, Annual Fall Meeting 2013, December 09–13, San Francisco, CA, USA, Geophysical Abstracts #G13B-0950
- Schupler B, Clark TA (1991) How different antennas affect the GPS observables. *GPS World* 2(10):32–36
- Schupler BR (2001) The response of GPS antennas: how design, environment and frequency affect what you see. *Phys Chem Earth A Solid Earth Geod* 26(6–8):605–611. doi:[10.1016/S1464-1895\(01\)00109-0](https://doi.org/10.1016/S1464-1895(01)00109-0)
- Schupler BR, Clark TA (2001) Characterizing the behavior of geodetic GPS antennas. *GPS World* 12(2):48–55
- Seeber G (2003) Satellite geodesy. Walter de Gruyter, Berlin. doi:[10.1515/9783110200089](https://doi.org/10.1515/9783110200089)
- Seeber G, Böder V (2002) Entwicklung und Erprobung eines Verfahrens zur hochpräzisen Kalibrierung von GPS Antennenaufstellungen - Schlussbericht zum BMBF/DLR Vorhaben 50NA9809/8. Institut für Erdmessung
- Seeber G, Menge F, Völkens C, Wübbena G, Schmitz M (1997a) Precise GPS positioning improvements by reducing antenna and site dependent effects. Scientific assembly of the international association of geodesy IAG97, September 03–09. Rio de Janeiro, Brasil
- Seeber G, Menge F, Völkens C, Wübbena G, Schmitz M (1997b) Precise GPS positioning improvements by reducing antenna and site dependent effects. In: Brunner FK (ed) Advances in positioning and reference frames—IAG scientific assembly, September 3–9, Rio de Janeiro, Brasilia, volume 118 of international association of geodesy symposia, pp 237–244. doi:[10.1007/978-3-662-03714-0_38](https://doi.org/10.1007/978-3-662-03714-0_38)
- Sims ML (1985) Phase center variation in the geodetic TI 4100 GPS receiver system's conical spiral antenna. In: Goad CC (ed) Proceedings of the first international symposium on precise positioning with the global positioning system, April 15–19, Rockville, MD, USA, vol 1, pp 227–244
- Steigenberger P, Rothacher M, Schmid R, Rülke A, Fritsche M, Dietrich R, Tesmer V (2007) Effects of different antenna phase center models on GPS-derived reference frames. In: Drewes H (ed) Geodetic Reference Frames, IAG Symposia, vol 134. Springer, Berlin, pp 83–88. doi:[10.1007/978-3-642-00860-3_13](https://doi.org/10.1007/978-3-642-00860-3_13)
- Tatarnikov DV, Astakhov AV (2013) Large impedance ground plane antennas for mm-accuracy of GNSS positioning in real time. In: Progress electromagnetics research symposium, August 12–15. Stockhol, Schweden, pp 1825–1829
- Tranquilla JB, Colpitts BG (1989) GPS antenna design characteristics for high-precision applications. *J Surv Eng ASCE* 115(1):2–14. <http://hdl.handle.net/1882/24113>
- Tranquilla JM, Carr JP, Hussain MA (1994) Analysis of a choke ring ground plane for multipath control in global positioning system (GPS) applications. *IEEE Trans Antennas Propagat* 42(7):905–911. doi:[10.1109/8.299591](https://doi.org/10.1109/8.299591)
- van Graas F, Bartone C, Arthur T (2004) GPS antenna phase and group delay corrections. In: Institute of Navigation (ION), National Technical Meeting (NTM) 2004, January 26–28, San Diego, CA, USA. Institute of Navigation (ION), pp 399–408
- Wanninger L (2009) Correction of apparent position shifts caused by GNSS antenna changes. *GPS Solut* 13(2):133–139. doi:[10.1007/s10291-008-0106-z](https://doi.org/10.1007/s10291-008-0106-z)
- Wirola L, Kontola I, Syrjärinne J (2008) The effect of the antenna phase response on the ambiguity resolution. In: Proceedings of the position, location and navigation symposium 2008, ION/IEEE, May 5–8, Monterey, CA, USA, pp 606–615. doi:[10.1109/PLANS.2008.4570104](https://doi.org/10.1109/PLANS.2008.4570104)
- Wübbena G (1985) Software developments for geodetic positioning with GPS using TI 4100 code and carrier measurements. In: Goad CC (ed) Proceedings of the first international symposium on precise positioning with the global positioning system, April 15–19, Rockville, MD, USA, vol 1. International Union of Geodesy and

- Geophysics, International Association of Geodesy, U.S. Department of Defense and U.S. Department of Commerce, pp 403–412
- Wübbena G, Menge F, Schmitz M, Seeber G, Völksen C (1996) A new approach for field calibration of absolute antenna phase center variations. In: Proceedings of the 9th international technical meeting of the Satellite Division of The Institute of Navigation (ION GPS 1996), September 17–20. Kansas City, MO, pp 1205–1214
- Wübbena G, Schmitz M, Menge F, Böder V, Seeber G (2000) Automated absolute field calibration of GPS antennas in real-time. In: Proceedings of the 13th international technical meeting of the Satellite Division of The Institute of Navigation (ION GPS 2000), September 19–22., Salt Lake City, UT, USA. Institute of Navigation (ION), pp 2512–2522
- Wübbena G, Schmitz M, Menge F, Seeber G, Völksen C (1997) A new approach for field calibration of absolute antenna phase center variations. *Navigation* 44(2):247–256
- Wübbena G, Schmitz M, Propp M (2008) Antenna group delay calibration with the Geo++ Robot—extensions to code observable. IGS Analysis Workshop, June 2–6. Miami Beach, FL, USA
- Zeimetz P (2010) Zur Entwicklung und Bewertung der absoluten GNSS-Antennenkalibrierung im HF-Labor. Ph.D. thesis, Institut für Geodäsie und Geoinformation, Universität Bonn. <http://hss.ulb.uni-bonn.de/2010/2212/2212.pdf>